Grain boundary segregation and thermodynamically stable binary nanocrystalline alloys

Jason R. Trelewicz and Christopher A. Schuh
Department of Materials Science and Engineering, Massachusetts Institute of Technology, 77 Massachusetts Avenue, Cambridge, Massachusetts 02139, USA

(Received 23 December 2008; revised manuscript received 19 January 2009; published 24 March 2009)

A free-energy function for binary polycrystalline solid solutions is developed based on pairwise nearest-neighbor interactions. The model permits intergranular regions to exhibit unique energetics and compositions from grain interiors, under the assumption of random site occupation in each region. For a given composition, there is an equilibrium grain size, and the alloy configuration in equilibrium generally involves solute segregation. The present approach reduces to a standard model of grain boundary segregation in the limit of infinite grain size, but substantially generalizes prior thermodynamic models for nanoscale alloy systems. In particular, the present model allows consideration of weakly segregating systems, systems away from the dilute limit, and is derived for structures of arbitrary dimensionality. A series of solutions for the equilibrium alloy configuration and grain size are also presented as a function of simple input parameters, including temperature, alloy interaction energies, and component grain boundary energies.

DOI: 10.1103/PhysRevB.79.094112 PACS number(s): 61.46.−w, 61.72.Mm, 64.75.Gh

I. INTRODUCTION

A variety of unique properties emerge as the characteristic microstructural length scale of a polycrystalline material is reduced to the nanometer range.[1–8] The resulting structures are composed of a high volume fraction of internal interfaces, which represent an interesting class of materials with opportunities that extend to emerging technologies, and also provide a platform for studying interface-dominated physics. However, the introduction of a high density of interfaces has an associated energetic penalty, and nanocrystalline materials tend to be unstable with respect to thermally activated structural changes.[9–11] The problem of nanostructure stability is most apparent in elemental nanocrystalline metals, such as Ni,[2] Cu,[12–16] Al,[17,18] and Pd,[19,20] which exhibit grain growth at very low homologous temperatures. These materials occupy a far-from-equilibrium state, which can be understood in the thermodynamic context formalized by Gibbs. The change in the Gibbs free energy, G, with respect to grain boundary area, A, is proportional to the grain boundary energy, γ.

$$dG \propto \gamma dA. \tag{1}$$

An elemental metal has a positive grain boundary energy, so a reduction in the interfacial area (i.e., an increase in grain size) will always lower the Gibbs free energy.

Alloying has the potential to suppress the instability of pure nanocrystalline materials, as evidenced by the enhanced thermal stability of a number of binary nanocrystalline alloys relative to their single-component counterparts.[14,21–24] While such behavior has been traditionally linked to kinetic phenomena such as solute drag,[25] recent studies have suggested that nanocrystalline alloys could in fact be thermodynamically stabilized by solute enrichment at the grain boundaries.[26–28] The idea of segregation-induced thermodynamic stability in nanocrystalline solids was first addressed analytically by Weissmüller,[28–30] who considered the change in the Gibbs free energy of a polycrystal upon alloying. Under certain simplifying assumptions, a minimum free energy is predicted at a specific solute content for a given grain size. This critical segregant level can be physically interpreted as the amount required to fill the available grain boundary sites without supersaturating the interface. By solving the Gibbs adsorption equation in the dilute limit assuming McLean-type segregation,[31] the grain boundary energy takes the following form:[28]

$$\gamma = \gamma_o - \Gamma|_{X\to 0, f_{ig}\to 0}(H_{seg} + kT \ln X). \tag{2}$$

Here γ_o is the grain boundary energy of the pure solvent, X is the global solute content, $\Gamma|_{X\to 0, f_{ig}\to 0}$ is the solute excess in the grain boundary (where the subscripts denote the limiting assumptions with f_{ig} the interfacial volume fraction), H_{seg} is the segregation energy (i.e., the difference in energy of a solute atom occupying a grain boundary site vs a grain interior site), k is the Boltzmann constant, and T is absolute temperature. From Eq. (2), it is evident that the grain boundary energy can be reduced by enhancing the solute excess, and if the magnitude of this reduction is sufficient to drive γ to zero, the grain boundaries can apparently exist in equilibrium.

Extremely fine nanocrystalline grain sizes have been realized in a variety of binary alloy systems, for example Y-Fe,[32] Ni-P,[33] Pd-Zr,[27,34] and Fe-Zr.[35] Because the elements composing these alloys are highly immiscible with a large positive heat of mixing, these systems are classified as strongly segregating, with high assumed values of H_{seg} ($\geq$0.5 eV) that can substantially reduce the grain boundary energy via Eq. (2). In all the alloy systems identified above, higher alloy compositions have been experimentally correlated with finer grain sizes (i.e., a higher volume fraction of grain boundaries), suggesting grain boundary segregation as the essential driving force for nanostructure stabilization. Alloys with a weaker apparent segregation tendency have also been synthesized with grain sizes spanning the entire nanocrystalline regime. An example in this regard is the Ni-W system, where there is some solid solubility, the segregation energy is low ($\sim$0.1 eV) and reduces further with increasing solute (W)

addition;[36] nevertheless, any grain size in the nanocrystalline range can be produced by controlling the solute content.[37]

For some of the binary alloy systems discussed above, solute enrichment at grain boundaries has been confirmed by atom probe tomography.[38–41] It has also been studied extensively by computer simulations both for individual grain boundaries[42] and, more recently, for simulated nanocrystalline structures.[36,43,44] A particularly clear illustration of the principle behind Eq. (2) is provided by the molecular-dynamics simulations of Millet *et al.*,[44] which explicitly show that for artificial states of segregation in Lennard-Jones polycrystals, the grain boundary energy can indeed be driven to zero.

Complementary analytical models have sought to extend the early work of Weissmüller[28] to understand the nature of grain boundary energy reduction and solute distributions in terms of the unique thermodynamic properties of binary nanocrystalline systems.[26,33,45–47] However, the key assumptions used in most of these models are quite severe, and generally limit the discussion to dilute solutions with extremely high segregation tendencies. This is unfortunate because most of the experimental nanocrystalline alloys described earlier are nondilute, and not all of them exhibit a strong tendency for segregation (e.g., Ni-W). Recently, Beke *et al.*[48,49] relaxed some of these assumptions in a statistical model, and considered segregation to free surfaces on one-dimensional nanocrystals. The statistical nature of this model is attractive in principle, providing a concrete framework to evaluate the conditions for equilibrium directly from a free-energy function. However, being derived for segregation to a free surface, this model lacks some of the thermodynamic parameters associated with grain boundary properties that are essential in differentiating various nanocrystalline alloys.

Thus, despite the progress cited above, there is as yet no simple analytical model for grain boundary segregation-based nanostructure stabilization that extends to general (nondilute) alloys, and incorporates energetic interactions that derive from the characteristic thermodynamic quantities governing the mixing behavior of binary systems. In this paper, we formulate such an analytical thermodynamic model, without restricting ourselves to the dilute limit or to strongly segregating solute species. The derivation is presented for grain geometries of arbitrary dimensionality, and includes interactions among segregated solute atoms, which alleviates the need to assume saturated grain boundaries. The result is a simple model that permits comparative analysis of various binary alloys and provides improved guidelines for design of nanocrystalline materials.

II. ANALYTICAL FRAMEWORK

In this section, the statistical framework required to analyze grain boundary segregation in binary alloy systems is developed. We begin by presenting a modified form of the regular solution model that captures the additional energetic penalty associated with introducing internal interfaces (i.e., grain boundaries) of a finite volume fraction into a single-phase crystalline solution. The possibility of any competing secondary or intermetallic phases is explicitly neglected, as are contributions from any additional thermodynamic potentials. The enthalpy of mixing is formulated by incorporating the distribution of bonds in the grains and intergranular regions into a modified solution model, and combined with entropic contributions to establish the free energy of mixing. A series of equilibrium equations are finally derived from the free-energy function, which can be used to investigate thermodynamically stable grain sizes.

TABLE I. Bulk, intergranular, and transitional bond configurations and their corresponding energies. Note that transitional bonds are assigned energies characteristic of the intergranular region.

Region	Number	Energies
Bulk	N_b^{AA}	E_b^{AA}
	N_b^{BB}	E_b^{BB}
	N_b^{AB}	E_b^{AB}
Intergranular	N_{ig}^{AA}	E_{ig}^{AA}
	N_{ig}^{BB}	E_{ig}^{BB}
	N_{ig}^{AB}	E_{ig}^{AB}
Transitional	N_t^{AA}	E_{ig}^{AA}
	N_t^{BB}	E_{ig}^{BB}
	N_t^{AB}	E_{ig}^{AB}

A. Solution model

To describe a binary mixture of solvent "A" and solute "B" atoms, we consider a statistical framework that employs pairwise interaction energies in a manner analogous to that which yields the regular solution model. However, we divide the full volume of the system into two separate regions—that belonging to the grains, and that belonging to intergranular regions. The latter region shall represent energetic contributions from all intergranular structural elements, including grain boundaries, triple junctions, and quadruple nodes, which are averaged together in this construction. The atomic interactions are uniquely defined in the bulk and intergranular regions, as illustrated in Table I. It also becomes necessary to introduce additional bonding pairs to capture bonds that bridge between the two distinct regions, as depicted in Fig. 1; we define these "transitional" bonds to have pairwise energies characteristic of the intergranular region (cf. Table I). The solution energy can be written as a sum over the individual bond energies, E, of all the possible atomic pairs, N, in each bonding region, r;

$$U_{\text{soln}} = \sum_r \{N_r^{AA}E_r^{AA} + N_r^{BB}E_r^{BB} + N_r^{AB}E_r^{AB}\}, \tag{3}$$

where the superscripts denote the bond types involved, and the subscript "r" distinguishes bulk (b), intergranular (ig), and transitional (t) bonds; all the possible bonding configurations are shown in Table I. Within this framework, the energy of mixing, ΔU_{mix}, not only accounts for chemical interactions in the solid solution, but also incorporates the interfacial energy characteristic of the intergranular region,

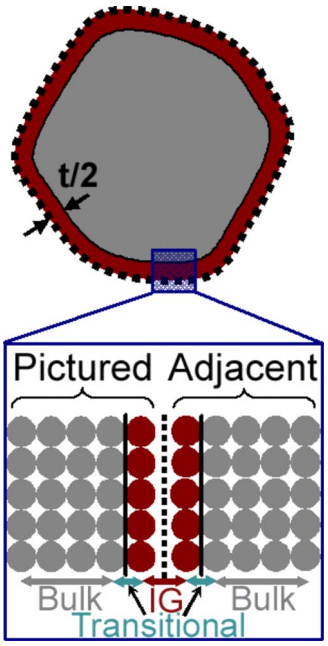

FIG. 1. (Color online) Schematic of an arbitrary grain shape, with the atomic configuration at the interface between the pictured and adjacent grain highlighted. Intergranular bonds are those located entirely within the intergranular region, and transitional bonds connect these atoms to those in the bulk region.

$$\Delta U_{\mathrm{mix}} = U_{\mathrm{soln}} - U_{\mathrm{ref}}, \tag{4}$$

where U_{ref} represents the energy of an unmixed, interface-free state of the same composition,

$$U_{\mathrm{ref}} = \left(\frac{zN^{\mathrm{A}}}{2}\right)E_{\mathrm{b}}^{\mathrm{AA}} + \left(\frac{zN^{\mathrm{B}}}{2}\right)E_{\mathrm{b}}^{\mathrm{BB}}. \tag{5}$$

The coordination number is denoted by z, and N^{A} and N^{B} are the total numbers of A and B atoms in solution, respectively.

For a system with a given global composition, the total number of each atom type is related to the number of bonds via

$$zN^{\mathrm{A}} = 2N_{\mathrm{b}}^{\mathrm{AA}} + 2N_{t}^{\mathrm{AA}} + 2N_{\mathrm{ig}}^{\mathrm{AA}} + N_{\mathrm{b}}^{\mathrm{AB}} + N_{t}^{\mathrm{AB}} + N_{\mathrm{ig}}^{\mathrm{AB}}, \tag{6a}$$

$$zN^{\mathrm{B}} = 2N_{\mathrm{b}}^{\mathrm{BB}} + 2N_{t}^{\mathrm{BB}} + 2N_{\mathrm{ig}}^{\mathrm{BB}} + N_{\mathrm{b}}^{\mathrm{AB}} + N_{t}^{\mathrm{AB}} + N_{\mathrm{ig}}^{\mathrm{AB}}, \tag{6b}$$

where the factors of 2 account for each like bond connecting two like atoms. We can express Eqs. (6a) and (6b) in terms of the numbers of like bonds in the bulk, and substitute these relations into Eqs. (3) and (5) to obtain the change in the internal energy upon mixing,

$$\begin{aligned}\Delta U_{\mathrm{mix}} = {} & N_{\mathrm{b}}^{\mathrm{AB}}\left(E_{\mathrm{b}}^{\mathrm{AB}} - \frac{E_{\mathrm{b}}^{\mathrm{AA}} + E_{\mathrm{b}}^{\mathrm{BB}}}{2}\right) + (N_{t}^{\mathrm{AA}} + N_{\mathrm{ig}}^{\mathrm{AA}})(E_{\mathrm{ig}}^{\mathrm{AA}} - E_{\mathrm{b}}^{\mathrm{AA}}) \\ & + (N_{t}^{\mathrm{BB}} + N_{\mathrm{ig}}^{\mathrm{BB}})(E_{\mathrm{ig}}^{\mathrm{BB}} - E_{\mathrm{b}}^{\mathrm{BB}}) + (N_{t}^{\mathrm{AB}} + N_{\mathrm{ig}}^{\mathrm{AB}}) \\ & \times\left(E_{\mathrm{ig}}^{\mathrm{AB}} - \frac{E_{\mathrm{b}}^{\mathrm{AA}} + E_{\mathrm{b}}^{\mathrm{BB}}}{2}\right),\end{aligned} \tag{7}$$

where terms involving the like bonding pairs in the bulk have cancelled with the equivalent terms contributed by the reference state. We now examine the geometric constraints imposed by a grain structure and the pairwise probabilities for forming the various bond types to determine explicit expressions for the seven remaining values of N in Eq. (7).

TABLE II. Bond configurations and existence probabilities, derived from the solute concentration in each of the respective regions, central to the free energy of mixing.

Region	Bonds	Energy	Probability	Bonds/ Region
Bulk	$N_{\mathrm{b}}^{\mathrm{AB}}$	$E_{\mathrm{b}}^{\mathrm{AB}}$	$2X_{\mathrm{b}}(1-X_{\mathrm{b}})$	P_{b}
Intergranular	$N_{\mathrm{ig}}^{\mathrm{AA}}$	$E_{\mathrm{ig}}^{\mathrm{AA}}$	$(1-X_{\mathrm{ig}})^2$	P_{ig}
	$N_{\mathrm{ig}}^{\mathrm{BB}}$	$E_{\mathrm{ig}}^{\mathrm{BB}}$	X_{ig}^2	
	$N_{\mathrm{ig}}^{\mathrm{AB}}$	$E_{\mathrm{ig}}^{\mathrm{AB}}$	$2X_{\mathrm{ig}}(1-X_{\mathrm{ig}})$	
Transitional	N_{t}^{AA}	$E_{\mathrm{ig}}^{\mathrm{AA}}$	$(1-X_{\mathrm{b}})(1-X_{\mathrm{ig}})$	P_{t}
	N_{t}^{BB}	$E_{\mathrm{ig}}^{\mathrm{BB}}$	$X_{\mathrm{b}}X_{\mathrm{ig}}$	
	N_{t}^{AB}	$E_{\mathrm{ig}}^{\mathrm{AB}}$	$X_{\mathrm{ig}}(1-X_{\mathrm{b}})+X_{\mathrm{b}}(1-X_{\mathrm{ig}})$	

B. Bond distributions

The number of bonds of each type present in each of the three bonding regions can be resolved by considering the total number of bonds inherent to each region, and the probability that each of these bonds is of a given type. To address the bonding distribution, we consider the volumetric density of atoms in each region, normalized by the total number of atoms in the system. Given an arbitrary grain geometry, the intergranular region is assigned as a shell of finite thickness, $t/2$, with a geometrically similar shape to the grain; this is illustrated in Fig. 1 for a two-dimensional grain of irregular shape.

Normalizing the volumetric atomic density by the total number of atoms eliminates the numerical shape factor associated with any specific grain geometry, and the intergranular volume fraction, f_{ig}, can be expressed as

$$f_{\mathrm{ig}} = 1 - \left(\frac{d-t}{d}\right)^{D}, \tag{8}$$

where d is the grain size, and D is the dimensionality of the grain structure. $D=3$ should be used for a general three-dimensional polycrystal, while $D=2$ is useful for columnar or highly elongated grain structures and $D=1$ applies to lamellar or platelike grains. We can also uniquely define the solute content in the bulk, X_{b}, and intergranular, X_{ig}, regions, which are related to the global solute content, X, by a volume fraction-weighted average,

$$X = (1 - f_{\mathrm{ig}})X_{\mathrm{b}} + f_{\mathrm{ig}}X_{\mathrm{ig}}. \tag{9}$$

The probability of each possible bond configuration can be enumerated by assuming random site occupation based on the defined compositions in each of the regions, and are listed in Table II.

The total number of bonding pairs present in the bulk (P_{b}), intergranular (P_{ig}), and transitional regions (P_t) are functions of f_{ig} and the total number of atoms, N_{o},

$$P_{\mathrm{b}} = \frac{z}{2}(1 - f_{\mathrm{ig}})N_{\mathrm{o}}, \tag{10a}$$

$$P_{\mathrm{ig}} = \left(\frac{z}{2}f_{\mathrm{ig}} - z\upsilon f_{\mathrm{ig}}\right)N_{\mathrm{o}}, \tag{10b}$$

$$P_t = z\upsilon f_{\mathrm{ig}}N_{\mathrm{o}}. \tag{10c}$$

According to Eq. (10a), the number of bulk bonds is simply equal to the total number of bonds in the system, $zN_{\mathrm{o}}/2$, weighted by the bulk volume fraction. The leading term in Eq. (10b) has the same form, weighting the total number of system bonds by the grain boundary volume fraction; the second term subtracts off the number of transitional bonds, which are counted separately in Eq. (10c). The factor, υ, termed the transitional bond fraction, represents the effective coordination for atoms contributing bonds to the transitional bonding region, and will be taken for all subsequent numerical calculations as 1/2. This essentially assigns half the atomic bonds at the bulk-intergranular interface as transitional bonds, with type probabilities deriving from both the bulk and intergranular solute fractions. When the occupation probabilities shown in Table II are scaled by the respective number of regional bonds, expressions for the seven bonding pairs central to the change in internal energy upon mixing are obtained.

C. Free-energy function

The free energy of mixing, ΔG_{mix}, is a combination of enthalpic and entropic contributions expressed as

$$\Delta G_{\mathrm{mix}} = \Delta H_{\mathrm{mix}} - T\Delta S_{\mathrm{mix}}, \tag{11}$$

where ΔH_{mix} and ΔS_{mix} represent the system enthalpy and entropy of mixing, respectively. As is customary for condensed phases, we neglect the change in volume upon mixing, and the enthalpy of mixing is thus represented by the change in internal energy given by Eq. (7), i.e., $\Delta H_{\mathrm{mix}} = \Delta U_{\mathrm{mix}}$. The entropy of mixing may be derived using the standard statistical approach, considering the random distribution of atoms over distinct atomic sites throughout the system, and simplifies to a volume fraction-weighted average of the random mixing entropy for the bulk and intergranular regions,

$$\Delta S_{\mathrm{mix}} = -kN_{\mathrm{o}}\{(1 - f_{\mathrm{ig}})[X_{\mathrm{b}}\ln X_{\mathrm{b}} + (1 - X_{\mathrm{b}})\ln(1 - X_{\mathrm{b}})] + f_{\mathrm{ig}}[X_{\mathrm{ig}}\ln X_{\mathrm{ig}} + (1 - X_{\mathrm{ig}})\ln(1 - X_{\mathrm{ig}})]\}. \tag{12}$$

Because the enthalpy and entropy of mixing both scale with system size, the free energy can be expressed on a per atom basis by normalizing with respect to N_{o}. Introducing Eqs. (7) and (12) into Eq. (11) yields the complete form of the free energy of mixing for our system. However, before introducing this full functional form, it is useful to examine the physical limits on grain size, which is bounded by $0 \le f_{\mathrm{ig}} \le 1$, corresponding to $t \le d \le \infty$. For $d \to \infty$, the free energy of mixing takes the form,

$$\Delta G^{\mathrm{b}}_{mix} = zX_{\mathrm{b}}(1 - X_{\mathrm{b}})\left(E^{\mathrm{AB}}_{\mathrm{b}} - \frac{E^{\mathrm{AB}}_{\mathrm{b}} + E^{\mathrm{AB}}_{\mathrm{b}}}{2}\right) + kT[X_{\mathrm{b}}\ln X_{\mathrm{b}} + (1 - X_{\mathrm{b}})\ln(1 - X_{\mathrm{b}})], \tag{13}$$

where X_{b} and X are equivalent via Eq. (9). As expected, in the infinite grain-size limit the free energy of mixing converges to a regular solution model for the bulk phase, and the combination of bond energies in Eq. (13) is accordingly recognized as the regular solution interaction energy:

$$\omega_{\mathrm{b}} = \left(E^{\mathrm{AB}}_{\mathrm{b}} - \frac{E^{\mathrm{AA}}_{\mathrm{b}} + E^{\mathrm{BB}}_{\mathrm{b}}}{2}\right). \tag{14}$$

Equation (14) has important implications for bond preference in the bulk, where $\omega_{\mathrm{b}} = 0$ is characteristic of an ideal solution, $\omega_{\mathrm{b}} > 0$ prefers like bonds, and $\omega_{\mathrm{b}} < 0$ unlike bonds.

In the other limit, $d \to t$ represents the reduction in grain size to the so-called "amorphous limit," where only the intergranular region exists, with a corresponding free energy,

$$\Delta G^{\mathrm{ig}}_{\mathrm{mix}} = \frac{z}{2}(1 - X_{\mathrm{ig}})(E^{\mathrm{AA}}_{\mathrm{ig}} - E^{\mathrm{AA}}_{\mathrm{b}}) + \frac{z}{2}X_{\mathrm{ig}}(E^{\mathrm{BB}}_{\mathrm{ig}} - E^{\mathrm{BB}}_{\mathrm{b}}) + zX_{\mathrm{ig}}(1 - X_{\mathrm{ig}})\left(E^{\mathrm{AB}}_{\mathrm{ig}} - \frac{E^{\mathrm{AA}}_{\mathrm{ig}} + E^{\mathrm{BB}}_{\mathrm{ig}}}{2}\right) + kT[X_{\mathrm{ig}}\ln X_{\mathrm{ig}} + (1 - X_{\mathrm{ig}})\ln(1 - X_{\mathrm{ig}})] \tag{15}$$

and X_{ig} is now equivalent to X. This expression may essentially be regarded as a regular solution model for the intergranular material, and contains a characteristic regular solution parameter analogous to Eq. (14),

$$\omega_{\mathrm{ig}} = \left(E^{\mathrm{AB}}_{\mathrm{ig}} - \frac{E^{\mathrm{AA}}_{\mathrm{ig}} + E^{\mathrm{BB}}_{\mathrm{ig}}}{2}\right). \tag{16}$$

In addition, the differences in like bond energies between the grain and intergranular sites are incorporated by the first two terms in Eq. (15), and are proportional to the grain boundary energies of the pure solvent, γ_{A}, and solute, γ_{B}, phases,

$$\gamma_{\mathrm{A}} \propto \frac{z}{2}(E^{\mathrm{AA}}_{\mathrm{ig}} - E^{\mathrm{AA}}_{\mathrm{b}}), \tag{17a}$$

$$\gamma_{\mathrm{B}} \propto \frac{z}{2}(E^{\mathrm{BB}}_{\mathrm{ig}} - E^{\mathrm{BB}}_{\mathrm{b}}). \tag{17b}$$

Introducing these relations into Eq. (15), the resultant free energy in the $d \to t$ limit is written more succinctly as

$$\Delta G^{\mathrm{ig}}_{\mathrm{mix}} = \frac{\Omega}{t}(1 - X_{\mathrm{ig}})\gamma_{\mathrm{A}} + \frac{\Omega}{t}X_{\mathrm{ig}}\gamma_{\mathrm{B}} + zX_{\mathrm{ig}}(1 - X_{\mathrm{ig}})\omega_{\mathrm{ig}} + kT[X_{\mathrm{ig}}\ln X_{\mathrm{ig}} + (1 - X_{\mathrm{ig}})\ln(1 - X_{\mathrm{ig}})], \tag{18}$$

where the solvent atomic volume, Ω, normalized by the intergranular shell thickness is taken for the proportionality constants in Eq. (17). Interestingly, Eq. (18) suggests that the free energy of a binary intergranular region involves both the chemical mixing preference and a weighted average of the grain boundary energies of the pure components.

Making use of some the above definitions, but without carrying any of the simplifying assumptions, the full mixing free energy function is written,

$$\Delta G_{\mathrm{mix}} = (1-f_{\mathrm{ig}})\Delta G^{\mathrm{b}}_{\mathrm{mix}} + f_{\mathrm{ig}}\Delta G^{\mathrm{ig}}_{\mathrm{mix}} + z\upsilon f_{\mathrm{ig}}\left\{[X_{\mathrm{ig}}(X_{\mathrm{ig}}-X_{\mathrm{b}}) - (1-X_{\mathrm{ig}})(X_{\mathrm{ig}}-X_{\mathrm{b}})]\omega_{\mathrm{ig}} - \frac{\Omega}{zt}(X_{\mathrm{ig}}-X_{\mathrm{b}})(\gamma_{\mathrm{B}}-\gamma_{\mathrm{A}})\right\}. \tag{19}$$

The leading two terms represent a rule of mixtures over the free energies of the bulk and intergranular regions, given by Eqs. (13) and (18), respectively. The last term captures energetic contributions from the transitional bonds between the bulk and intergranular regions, demonstrating that the free energy of a polycrystalline binary solid solution derives from more complex interactions than those described by a simple rule of mixtures.

D. Equilibrium equations

The equilibrium condition is given by the simultaneous minimization of ΔG_{mix} with respect to the intergranular composition and grain size for a closed system (i.e., constant X),

$$\left.\frac{\partial \Delta G_{\mathrm{mix}}}{\partial X_{\mathrm{ig}}}\right|_{X} \rightarrow 0, \tag{20a}$$

$$\left.\frac{\partial \Delta G_{\mathrm{mix}}}{\partial f_{\mathrm{ig}}}\right|_{X} \rightarrow 0. \tag{20b}$$

If we apply only the condition of Eq. (20a), an expression for the characteristic segregation isotherm is obtained, which describes the solute distribution for a given grain size,

$$\frac{X_{\mathrm{ig}}}{1-X_{\mathrm{ig}}} = \frac{X_{\mathrm{b}}}{1-X_{\mathrm{b}}}\cdot \exp\left[\frac{\Delta H_{\mathrm{seg}}}{kT}\right] \tag{21}$$

with a segregation energy, ΔH_{seg}, that bears some resemblance to the classical Fowler-Guggenheim form,

$$\Delta H_{\mathrm{seg}} = z\left[\omega_{\mathrm{b}} - \omega_{\mathrm{ig}}\left(1-\frac{\upsilon}{1-f_{\mathrm{ig}}}\right) - \frac{\Omega}{zt}(\gamma_{\mathrm{B}}-\gamma_{\mathrm{A}})\left(1-\frac{\upsilon}{1-f_{\mathrm{ig}}}\right)\right] + 2zX_{\mathrm{ig}}\omega_{\mathrm{ig}}\left(1-\frac{\upsilon}{1-f_{\mathrm{ig}}}\right) - 2z[X_{\mathrm{b}}\omega_{\mathrm{b}} + \upsilon(X_{\mathrm{ig}}-X_{\mathrm{b}})\omega_{\mathrm{ig}}]. \tag{22}$$

The leading bracketed term in Eq. (22) is a combination of bond energies that describes McLean-type segregation for a free surface, with no segregated solute-solute interactions. The additional terms account for such interactions, which in the present model are functions of υ and f_{ig}, thus imparting a grain-size dependence on the effective coordination in the intergranular region.

The second equilibrium condition of Eq. (20b) is analogous to imposing $\gamma \rightarrow 0$, as the alloy grain boundary energy, γ, is directly related to the partial derivative,

$$\gamma = \frac{t}{\Omega}\cdot\frac{\partial \Delta G_{\mathrm{mix}}}{\partial f_{\mathrm{ig}}}, \tag{23}$$

where the scaling factor t/Ω is the reciprocal of the proportionality constant introduced in Eq. (18). To calculate corresponding equilibrium grain sizes for the solute distributions given by Eqs. (9) and (21), Eq. (20b) must be concurrently evaluated and introduced into Eq. (23),

$$\gamma = \gamma_{\mathrm{A}} - \frac{ztX_{\mathrm{ig}}}{\Omega}\left[\omega_{\mathrm{b}} - \omega_{\mathrm{ig}}\left(1-\frac{\upsilon}{1-f_{\mathrm{ig}}}\right) - \frac{\Omega}{zt}(\gamma_{\mathrm{B}}-\gamma_{\mathrm{A}})\left(1-\frac{\upsilon}{1-f_{\mathrm{ig}}}\right)\right] - \frac{zt}{\Omega}\left[(X_{\mathrm{b}}^2 - 2X_{\mathrm{b}}X_{\mathrm{ig}})\omega_{\mathrm{b}} + X_{\mathrm{ig}}^2\omega_{\mathrm{ig}}\left(1-\frac{\upsilon}{1-f_{\mathrm{ig}}}\right)\right] + \frac{zt\upsilon}{\Omega(1-f_{\mathrm{ig}})}\left[\{X_{\mathrm{ig}}(X_{\mathrm{ig}}-X_{\mathrm{b}}) + X_{\mathrm{b}}(1-X_{\mathrm{ig}})\}\omega_{\mathrm{ig}} + X_{\mathrm{b}}\frac{\Omega}{zt}(\gamma_{\mathrm{B}}-\gamma_{\mathrm{A}})\right] + \frac{tkT}{\Omega}\left[X_{\mathrm{ig}}\ln\left(\frac{X_{\mathrm{ig}}}{X_{\mathrm{b}}}\right) + (1-X_{\mathrm{ig}})\ln\left(\frac{1-X_{\mathrm{ig}}}{1-X_{\mathrm{b}}}\right)\right] = 0. \tag{24}$$

While Eq. (24) appears cumbersome at first glance, its form can be understood by considering a simplified system: one in which we assume a dilute solute concentration ($X \rightarrow 0$), a high segregation tendency ($\Delta H_{\mathrm{seg}} \gg kT$), and McLean-type segregation ($f_{\mathrm{ig}} \rightarrow 0$), assumptions that were central in the prior models of nanostructure stability by Weissmüller[28] and Liu and Kirchheim.[33] Under these simplifying conditions, with $\upsilon = 1/2$, the segregation energy (denoted in this limit as $\Delta H^{\mathrm{o}}_{\mathrm{seg}}$) and alloy grain boundary energy simplify to

$$\Delta H^{\mathrm{o}}_{\mathrm{seg}} = z\left[\omega_{\mathrm{b}} - \frac{\omega_{\mathrm{ig}}}{2} - \frac{\Omega}{2zt}(\gamma_{\mathrm{B}}-\gamma_{\mathrm{A}})\right], \tag{25a}$$

$$\gamma = \gamma_{\mathrm{A}} - \frac{tX_{\mathrm{ig}}}{\Omega}[\Delta H^{\mathrm{o}}_{\mathrm{seg}} + kT\ln(X_{\mathrm{b}})], \tag{25b}$$

where Eq. (25a) characterizes McLean-type segregation, as discussed above in reference to the leading term of Eq. (22). Equation (25b) is incorporated as the leading two terms of Eq. (24), and simplifies exactly to Eq. (2); the solute excess in the dilute, infinite grain-size limit is expressed as

$$\Gamma|_{X\rightarrow 0, f_{\mathrm{ig}}\rightarrow 0} = \frac{t\cdot X_{\mathrm{ig}}}{\Omega}, \tag{26}$$

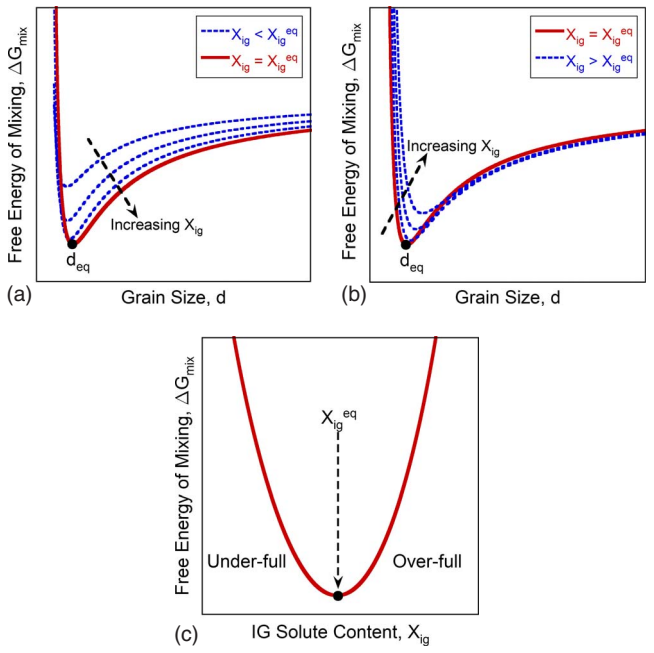

FIG. 2. (Color online) Two-dimensional slices of the free-energy surface as a function grain size for intergranular solute contents (a) less than and (b) greater than the equilibrium composition, X_{ig}^{eq}. For the equilibrium grain size indicated in (a) and (b), ΔG_{mix} is plotted in (c) as a function of intergranular solute content, and demonstrates a minimum at X_{ig}^{eq}; intergranular compositions less than or greater than X_{ig}^{eq} correspond to underfull or overfull boundaries, respectively. The minimum identified in the free energy of mixing represents the global minimum on the free-energy surface, and defines the thermodynamically stable state.

which is identical to the form provided in Ref. 33. Higher order effects from solute-solute and solute-solvent interactions in the bulk, transitional, and intergranular regions are captured by the remaining terms.

The true equilibrium state of a polycrystal is determined by simultaneously applying the two criteria of Eqs. (20), recast as Eqs. (21) and (24), and solving for the two unknowns, intergranular solute content and grain size. Because constant X is imposed, the equilibrium grain size is coupled to the global solute content, such that for any given composition there is one equilibrium grain size, and for any grain size there is one energy-minimizing composition. To illustrate this more clearly, we have schematically plotted ΔG_{mix}-d contours for various values of X_{ig} in Figs. 2(a) and 2(b) for a constant global composition. These plots are essentially two-dimensional projections of the free-energy surface as viewed along the X_{ig} axis, with Fig. 2(a) showing the approach to the minimum-energy configuration from below the equilibrium value of X_{ig}, and Fig. 2(b) showing the increase in system energy beyond. In each of the ΔG_{mix}-d contours there is a local minimum, but the true equilibrium grain size, d_{eq}, only exists on a single contour, corresponding to a single intergranular solute content, X_{ig}^{eq}, at the global minimum on the free-energy surface. The minimum in ΔG_{mix} with respect to X_{ig} can be more readily understood when plotted at the equilibrium grain size, as illustrated in Fig. 2(c). The free energy monotonically decreases when solute is

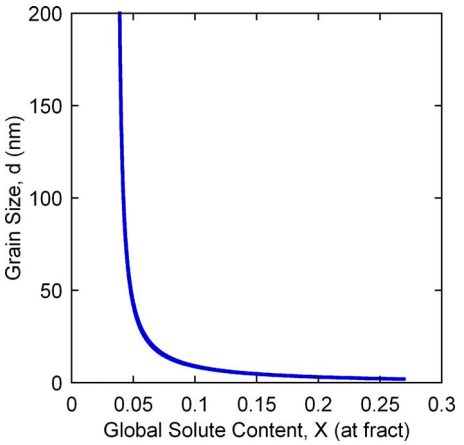

FIG. 3. (Color online) Equilibrium grain size as a function of the global solute content for a single example set of interaction energies. A power-law-like decay in grain size is observed with increasing global composition, indicating that more solute is required to stabilize finer nanocrystalline grain sizes.

initially added to the system, and in order to satisfy Eq. (21), enough solute must be supplied to minimize ΔG_{mix} as indicated. At lower solute contents, the grain boundaries can be viewed as "underfull" with additional sites available for solute atoms, whereas when X_{ig} surpasses the stable composition, the grain boundaries become saturated and solute atoms occupy energetically unfavorable sites in the bulk, resulting in the subsequent increase in ΔG_{mix}.

The minimization procedure described above can be employed to calculate equilibrium grain sizes and intergranular solute contents as a function of global composition for alloys with various interaction energies. The prototypical output of this model is illustrated in Fig. 3: the equilibrium grain size decreases with increasing global solute content in a power-law-like decay. The functional form of this relationship is a signature of thermodynamic stabilization, and is widely observed in experimental data on this subject.[27,32–34,37] Such scaling is an inherent consequence of Eq. (8), where the

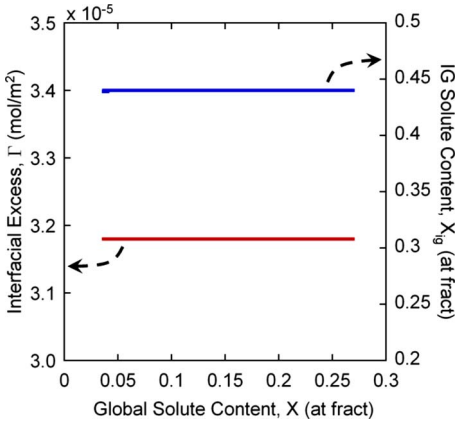

FIG. 4. (Color online) Interfacial excess and intergranular solute content plotted against the global solute content. For the example set of interaction energies, both quantities are independent of global composition, and thus denote the critical intergranular coverage level required to achieve equilibrium.

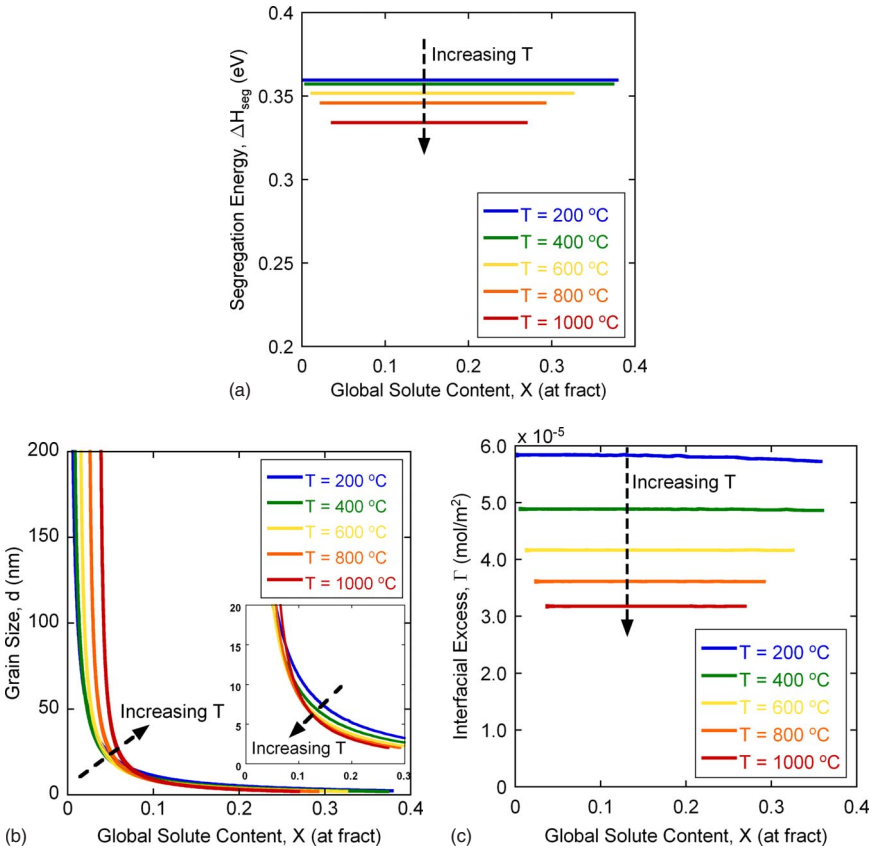

FIG. 5. (Color online) Thermodynamic equilibrium states as a function of temperature for interaction energies defined as: $\omega_b = 0.03$ eV, $\omega_{ig} = 0$ eV, and $\gamma_A = \gamma_B = 0.48$ J/m^2. With increasing temperature, (a) the segregation energy decreases, (b) the grain size trends first shift to higher solute contents, followed by a scaling inflection and shift to lower global compositions as shown in the inset, and (c) the interfacial excess decreases, indicating that temperature promotes a more random solute distribution.

grain boundary volume fraction is inversely related to grain size. Additional solute is thus required to effectively fill the grain boundaries and lower the system energy, especially at the finest nanocrystalline grain sizes where interfaces become the dominant structural feature.

While grain size correlates with the global composition, the corresponding segregation isotherm in Fig. 4 indicates that the intergranular composition is unaffected by solute additions. However, because d is coupled to X, the interfacial volume fraction varies with global composition, making it very difficult to analyze the segregation behavior from a characteristic isotherm. To address this complexity, we turn our attention to the Gibbsian excess, or intergranular solute excess, Γ,[31,50] which is derived by considering the distribution of atoms, N, in the system,

$$\Gamma = \frac{1}{A_{ig}}\left[N_{ig}^{B} - N_{b}^{B}\left(\frac{N_{ig}^{A}}{N_{b}^{A}}\right)\right]. \tag{27}$$

This representation is convenient as Γ is normalized by the interfacial area, A_{ig}, thus incorporating the inherent variation in interfacial volume fraction. A_{ig} can be calculated from the system volume, $N_0 \cdot \Omega$, and the intergranular volume faction and shell thickness,

$$A_{ig} = \frac{N_0 \cdot \Omega \cdot f_{ig}}{t}. \tag{28}$$

When Eq. (28) is introduced into Eq. (27), the interfacial excess takes the form

$$\Gamma = \frac{t(X_{ig} - X_b)}{\Omega(1 - X_b)}. \tag{29}$$

Note that this expression simplifies exactly to Eq. (26) in the dilute, infinite grain-size limit. Introducing the results for X_{ig}, X, and f_{ig} from the segregation isotherm into Eq. (29), we obtain Γ as a function of X, as illustrated in Fig. 4. As the segregation isotherms imply, the interfacial excess is indeed unaffected by solute additions for the given set of energetic state variables. However, this does not imply that Γ is universally independent of X, which is only observed here as a consequence of the chosen interaction energies. This will be demonstrated in the following parametric study, which will also emphasize the importance of incorporating grain-size variations when analyzing segregation behavior.

III. PARAMETRIC STUDY

The equilibrium equations derived in Sec. II are parameterized by a number of geometric and thermodynamic state variables that influence both the segregation tendency and equilibrium grain size, including T, ω_b, ω_{ig}, γ_A, γ_B, and D. In this section, we will illustrate the individual effects of these parameters by numerically evaluating Eqs. (21) and (24) to solve for equilibrium pairs of d and X, with an assumed constant intergranular shell thickness of $t = 0.5$ nm. The default settings of the state variables are the same throughout this section: $T = 1000$ °C, $\omega_b = 0.03$ eV (~2.9 kJ/mol), $\omega_{ig} = 0$ eV, $\gamma_A = \gamma_B = 0.48$ J/m^2, and $D = 3$; these values are used except where it is explicitly stated otherwise.

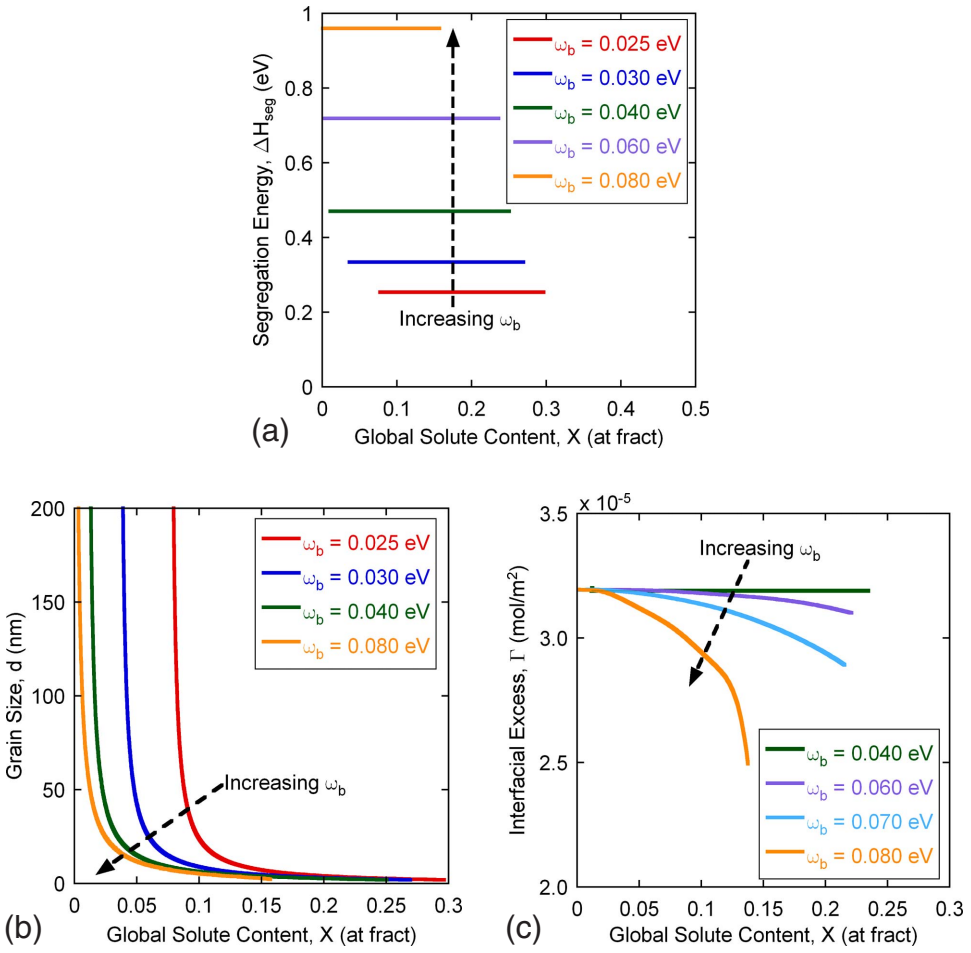

FIG. 6. (Color online) Thermodynamic equilibrium states as a function of the bulk interaction energy for the state variables: $T=1000\ ^\circ\mathrm{C}$, $\omega_{ig}=0$ eV, and $\gamma_A=\gamma_B=0.48\ \mathrm{J/m^2}$. With increasing bulk interaction energy, (a) the segregation energy increases and (b) the grain size trends shift to lower global solute contents, indicating that less solute is required to stabilize the nanostructure for large bulk interaction energies. (c) The interfacial excess is initially independent of composition at low ω_b, then scales with the global solute content as ω_b further deviates from ω_{ig}.

A. Temperature

Our free energy of mixing is derived for a system limited to pairwise nearest-neighbor interactions, an assumption that leads to a temperature-independent enthalpy, with T predominantly coupled to the entropy via Eq. (12). The most general influence of temperature, then, is to randomize the solute distribution, desegregating systems that exhibit a segregation tendency; this is captured in Fig. 5(a), where we have varied T over the range 200–1000 °C. Equilibrium grain size decreases with global composition in Fig. 5(b), and the temperature-dependent segregation energy affects this scaling in subtle and complex ways. First, for lower global compositions ($X<10$ at. %), the reduced driving force for segregation at elevated temperatures results in a lower interfacial excess, as evidenced in Fig. 5(c), and the system therefore requires more solute to effectively eliminate the alloy grain boundary energy; this is manifested in Fig. 5(b) as a shift of the d-X trends to higher global compositions. However, as X is increased beyond 10 at. %, the d-X trends instead shift to lower global compositions with increasing T, as demonstrated in the inset of Fig. 5(b). While this appears counterintuitive, the observed reduction in Γ [cf. Fig. 5(c)] indicates that the system transitions to a more random configuration with increasing X, which is favored at elevated temperatures. Less solute is required to achieve equilibrium in a more random system, thus accounting for the observed inflection in the scaling of the grain size-composition relationships with temperature.

B. Bulk interaction energy

The bulk interaction energy scales directly with the heat of mixing, which is viewed as one of the principal driving forces for grain boundary segregation. Here we examine the influence of ω_b over the range 0.025–0.08 eV. The segregation energy, shown in Fig. 6(a), markedly increases with increasing ω_b, as expected from Eq. (22); all other things being equal, higher heat-of-mixing alloys should exhibit a higher segregation tendency. The resulting effect on the equilibrium grain size-composition relationships is shown in Fig. 6(b); for greater values of ω_b, less global solute is required to stabilize a given nanocrystalline grain size, thereby shifting the characteristic d-X trends downward. However, the effect of ω_b on the interfacial excess, illustrated in Fig. 6(c), is more complex. For low bulk interaction energies ($\omega_b<0.05$ eV), the interfacial excess is independent of global composition, as illustrated in Fig. 6(c) for $\omega_b=0.04$ eV. Composition-independent Γ are also evident at even lower interaction energies, trending to reduced coverage levels as the system approaches an ideal solution (i.e., $\omega_b=0$), and are not included for clarity of presentation. As ω_b is increased beyond 0.05 eV, bulk atomic interactions more strongly dictate the segregation behavior, with like bond formation becoming more energetically favorable in the bulk. At higher global compositions where the probability to form like bonds is greatly enhanced, solute atoms prefer to occupy bulk sites to minimize the system free energy. This leads to a more

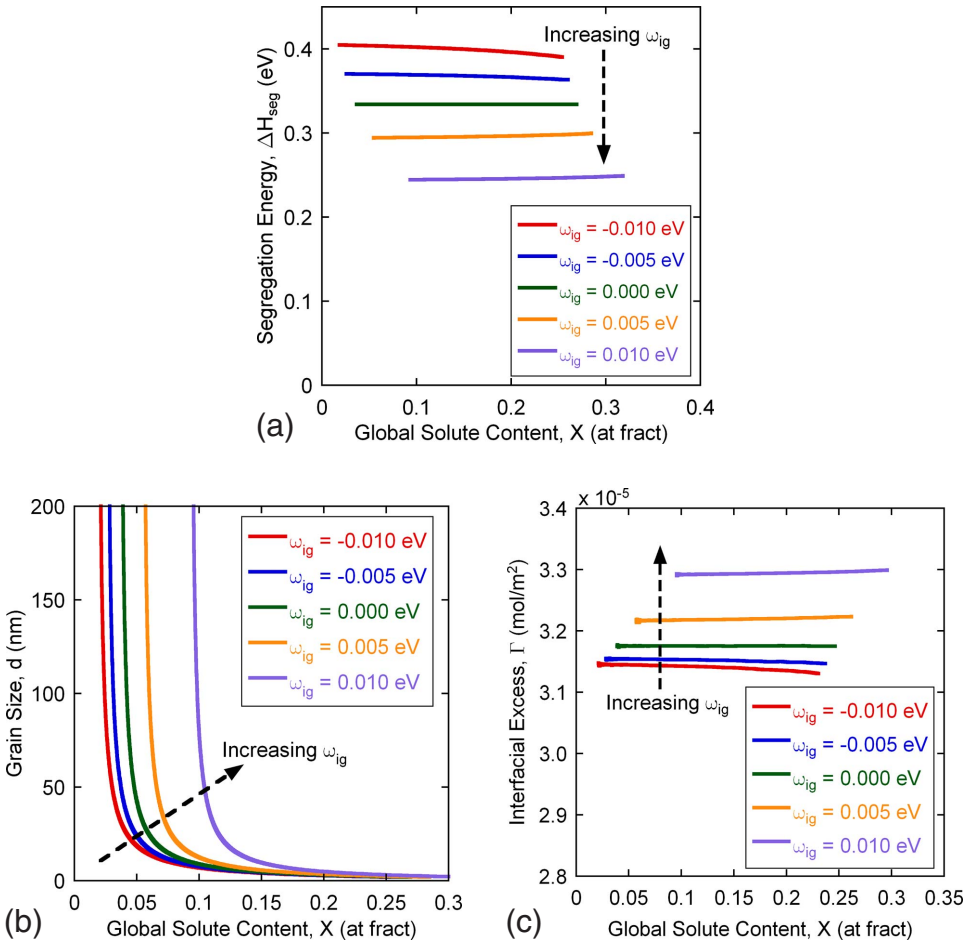

FIG. 7. (Color online) Thermodynamic equilibrium states as a function of the intergranular interaction energy for the state variables: $T=1000$ °C, $\omega_b=0.03$ eV, and $\gamma_A=\gamma_B=0.48$ J/m^2. With increasing intergranular interaction energy, (a) the segregation energy decreases, (b) the grain size trends shift to higher global solute contents, and (c) the interfacial excess increases toward higher coverage levels, all of which support that higher solute contents are required to stabilize the nanostructure as ω_{ig} tends toward large, positive values.

rapid decrease in Γ with increasing X, as observed in Fig. 6(c), especially when ω_b exceeds 0.06 eV.

C. Intergranular interaction energy

One of the essential features of the present model is its adaptability to a variety of alloy systems via distinct, tunable interaction energies. For clarity in evaluating the effect of T and ω_b in Secs. III A and III B, the intergranular region was assumed to behave as an ideal solution, with no particular bonding inclination. In this section, the intergranular interaction energy is varied and the results are contrasted with the effect of the bulk interaction energy. The equilibrium results are summarized in Fig. 7 as a function of ω_{ig}, and generally exhibit opposite trends as compared to the effect of ω_b. Figure 7(a) illustrates that as ω_{ig} is increased, a noticeable reduction in the driving force for segregation results, owing to the enhanced energetic penalty imparted on segregating atoms. The equilibrium d-X relationships, shown in Fig. 7(b), shift to higher global compositions to counteract the reduced driving force for segregation.

D. Solvent grain boundary energy

In this section, we systematically vary γ_A while γ_B is held constant at 0.48 J/m^2; whereas the driving force for segregation in Secs. III A–III C derived from the interaction energies of the bulk and intergranular regions, here the differential between the pure component grain boundary energies becomes a second-order contribution to the segregation energy. Because a greater energetic penalty is imposed on atoms occupying intergranular sites as γ_A is increased, the desire for solute atoms to segregate to the grain boundaries diminishes, with a corresponding decrease in ΔH_{seg} [Fig. 8(a)]. However, since equilibrium requires segregated solute to counteract the interfacial energy, more solute should be required to effectively eliminate a higher grain boundary energy, as is indeed observed in Figs. 8(b) and 8(c) via an upward shift of the d-X relationships and the interfacial excess with increasing γ_A. The segregation energy also varies with X for various values of γ_A, and specifically depends on the relative difference between γ_A and γ_B. When $\gamma_A > \gamma_B$, a decrease in the segregation energy is observed with increasing global composition, while the opposite trend is realized when $\gamma_A < \gamma_B$. For the case where $\gamma_A > \gamma_B$, an A-rich boundary is characterized by a higher energy and lower driving force for segregation, as discussed above, leading to the observed decrease in ΔH_{seg} with X. The converse case follows the same logic, and when $\gamma_A = \gamma_B$, the nature of the boundaries no longer influences the propensity for segregation, as illustrated by the composition-independent segregation energy in Fig. 8(a).

E. Grain structure dimensionality

The present model does not require specification of a distinct grain shape, but the dimensionality of the grains affects

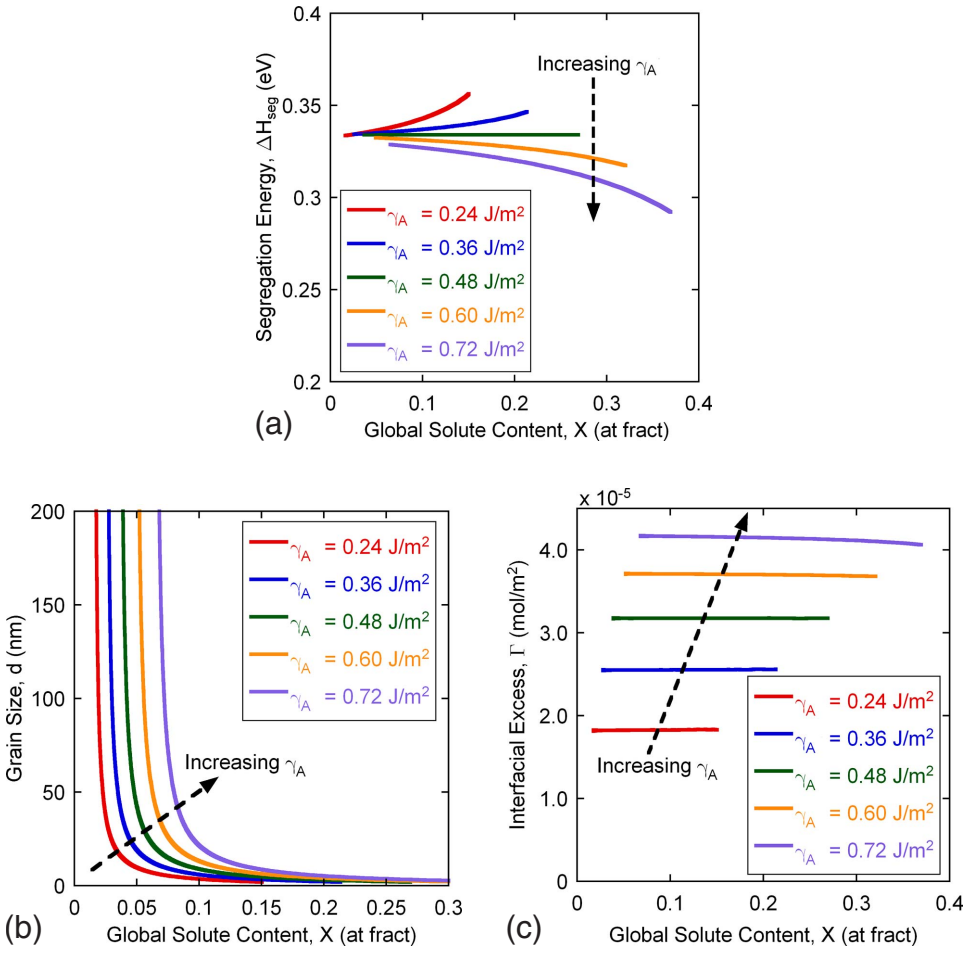

FIG. 8. (Color online) Thermodynamic equilibrium states as a function of the solvent grain boundary energy for the state variables: T=1000 °C, ω_b=0.03 eV, and ω_{ig}=0 eV. With increasing grain boundary energy, (a) the segregation energy generally decreases (but depends to a large extent on the global solute content and relative magnitudes of the solute-solvent grain boundary energies), (b) the grain size trends shift to higher global solute contents, and (c) the interfacial excess increases toward higher coverage levels. These observations indicate that more solute is required to drive higher energy grain boundaries to equilibrium.

the scaling of grain boundary volume fraction with grain size via Eq. (8), and thus impacts the final equilibrium state. For the chosen set of energetic state variables, the segregation energy is calculated to be 0.36 eV, and is independent of both dimensionality and global composition. However, the equilibrium grain size-global composition relationships are a function of grain dimension, as shown in Fig. 9(a). As D increases, the d-X curves shift to higher global compositions for the same solute distribution. According to Eq. (8), for a specified grain size and intergranular shell thickness, the intergranular volume fraction exponentially increases with grain dimension, and additional solute is therefore required to effectively eliminate the alloy grain boundary energy at higher f_{ig}. However, the critical interfacial excess required for $\gamma \rightarrow 0$ is independent of grain dimensionality, as shown in Fig. 9(b), and decreases with X to reduce the probability for energetically unfavorable solute-solute interactions in the grain boundary.

IV. IMPLICATIONS FOR EXPERIMENTAL NANOCRYSTALLINE ALLOYS

The present model is strictly limited to binary systems with no competing second phases, and considers only pairwise first-order interactions. Accordingly, it is not intended to directly predict behavior of specific alloy systems in a quantitative sense, where higher order atomic interactions and competing phases must be considered. However, it can offer some qualitative guidelines for understanding differences in the behavior of various binary alloys that have been studied extensively in the experimental literature. For example, consider electrodeposited alloys of Ni-W and Ni-P, which both exhibit the characteristic d-X trend expected for segregation-based stabilization, as shown in Fig. 10(a) after Detor and Schuh[37] and Liu and Kirchheim,[33,34] respectively. Whereas the experimental grain size-composition data for the Ni-P system exhibit a very limited range of accessible nanocrystalline grain sizes, with a rather sharp bend in the curve at ~3 at. % P, results for the Ni-W system demonstrate a much broader range of attainable grain sizes, with a more gradual increase in the slope as compared to Ni-P. Furthermore, atom probe tomography has demonstrated a rather subtle segregation tendency for Ni-W alloys,[38] while considerable segregation has been observed in Ni-P alloys.[39] Although these materials are deposited using a similar nonequilibrium approach, and experimental evidence suggests that they are not in a formally stable thermodynamic state, there is evidence that they are in a deep metastable condition with a strong thermodynamic contribution to their stability.[21,26] Moreover, since they are both produced by essentially similar methods, they should be in comparable states, permitting some comparison of their very different characteristic curves in Fig. 10(a) on the basis of alloy energetics.

Thermodynamic data, such as solution interaction energies (i.e., ω_b), are readily available for binary systems;

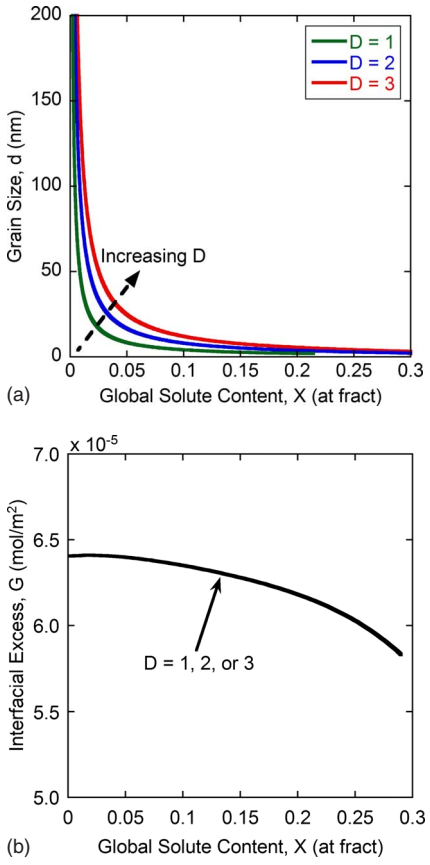

FIG. 9. (Color online) (a) Equilibrium grain size vs global composition as a function of grain structure dimensionality. (b) Interfacial excess plotted for $D=1$, 2, or 3 as a function of global solute content. The trends in (a) shift to higher global solute contents as D increases, attributed to the concurrent increase in grain boundary volume fraction. The interfacial excess in (b) is independent of dimensionality, and its functional dependence on X is imparted by the assigned state variables: $T=1000$ °C, $\omega_b=0.03$ eV, $\omega_{ig}=0$ eV, $\gamma_A=\gamma_B=0.48$ J/m^2.

for Ni-W in particular, ω_b is on the order of 0.05 eV when considering only first-order interactions, which is roughly a sixth (i.e., $2/z$) the magnitude of the heat of mixing ($\sim$0.27 eV/atom) as determined via Miedema's semiempirical mixing model.[51–53] Similarly, for Ni-P we approximate $\omega_b \approx 0.1$ eV by scaling the heat of mixing from Miedema's model by $2/z$. Employing these interaction energies and assuming $\omega_{ig} \approx \omega_b$, $T=100$ °C (close to the deposition temperature), and $\gamma_A=\gamma_B=0.5$ J/m^2, we computed d-X trends for Ni-W and Ni-P-like interactions, as illustrated in Fig. 10(b). Whereas the d-X relationship for ω_b of 0.1 eV exhibits a relatively sharp increase in grain size at a low global solute content, as demonstrated in Fig. 10(b) and similar to the Ni-P data in Fig. 10(a), the 0.05 eV interaction energy trend is shifted to higher global solute contents with a more moderate curvature, in line with the Ni-W experimental results. The difference between these curves is a consequence of the higher-order terms in Eq. (24), where solute-solute and solute-solvent interactions in the grain boundary tend to ease the rate at which γ decreases, thus shifting the equilibrium trends to higher global solute contents.

This example illustrates how differences in alloy energetics can influence the formation and stabilization of nanocrystalline structures. On the one hand, we may conclude that more pronounced atomic interactions in the bulk (i.e., a high bulk heat of mixing) correlate with a higher grain boundary segregation tendency, which leads to more rapid grain refinement at small solute additions. On the other hand, a lower bulk interaction energy (lower heat-of-mixing) system requires more solute to achieve the same grain size, and thus has a more gently sloping d-X curve as in Fig. 10(b); this may offer more precise control over grain size than would the steeper trend found in more strongly segregating systems, where slight compositional fluctuations lead to large deviations in grain size.

V. CONCLUSIONS

Within the framework of statistical thermodynamics, we have developed an analytical model for nanostructure stabi-

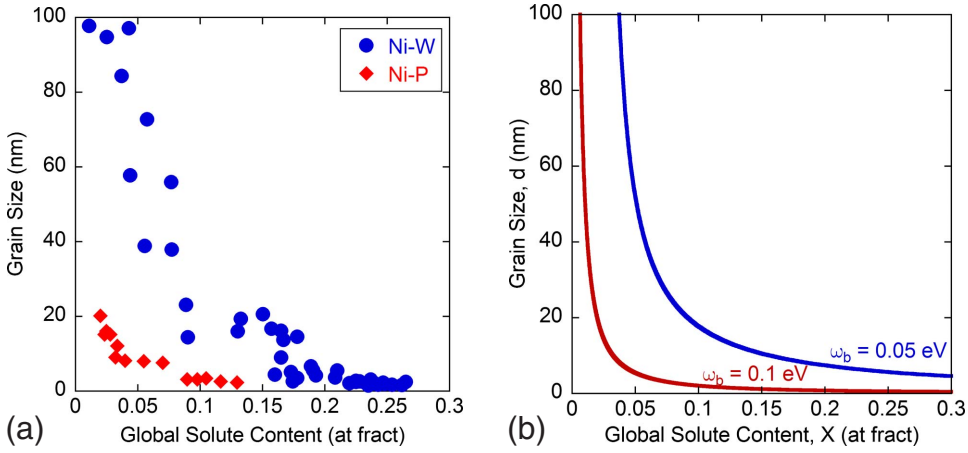

FIG. 10. (Color online) (a) Experimental grain size-composition data for the strongly segregating Ni-P system and the weakly segregating Ni-W system, after Liu and Kirchheim (Ref. 33) and Detor and Schuh (Ref. 37), respectively. A higher alloy composition promotes finer grain sizes, regardless of the segregation tendency. (b) Grain size as a function of global composition for systems modeled after Ni-P with $\omega_b=0.1$ eV, and Ni-W with $\omega_b=0.05$ eV. The Ni-W-like trend is shifted to higher global solute contents, with a more gradual increase in grain size with decreasing composition, as compared to the Ni-P-like trend.

lization in binary systems, extending previous models to more general segregation behavior and alloy compositions. The result is essentially a regular solution model for a binary polycrystalline system, in which grain size is a state variable and grain boundary segregation contributes strongly to the energetics of the system. Global energetic variables are identified from the various bonds (A-A, B-B, and A-B) in grain interiors and grain boundaries, and their influence on the equilibrium states were investigated in a parametric study, revealing that:

(i) In binary systems, segregation of solute to grain boundaries leads to an equilibrium grain size at which the system energy is minimized, as suggested by prior models. The equilibrium grain size decreases as solute is added to the system.

(ii) A reduced segregation energy is exhibited by systems with a lower bulk interaction energy, higher intergranular interaction energy, and a higher solvent grain boundary energy.

(iii) Lower segregation energies generally shift the equilibrium grain size-composition trends upward (to higher global compositions), and promote a gentler decrease in grain size with increasing global solute content.

(iv) All other things being equal, temperature acts to randomize the solute distribution, generally shifting the grain size-composition trends upward, to higher global solute contents.

The model offers some insight on differences between various experimental alloys, and also offers guidance for the selection of alloying elements that promote nanocrystalline structures.

ACKNOWLEDGMENTS

This work was primarily supported by the U.S. National Science Foundation under Grant No. DMI-0620304, with partial support of the U.S. Army Research Office.

[1] G. Herzer, Scr. Metall. Mater. **33**, 1741 (1995).
[2] L. Lu, Y. F. Shen, X. H. Chen, L. H. Qian, and K. Lu, Science **304**, 422 (2004).
[3] T. Suzuki, I. Kosacki, V. Petrovsky, and H. U. Anderson, J. Appl. Phys. **91**, 2308 (2002).
[4] A. S. Argon and S. Yip, Philos. Mag. Lett. **86**, 713 (2006).
[5] H. Gleiter, Acta Mater. **48**, 1 (2000).
[6] K. S. Kumar, H. Van Swygenhoven, and S. Suresh, Acta Mater. **51**, 5743 (2003).
[7] M. A. Meyers, A. Mishra, and D. J. Benson, Prog. Mater. Sci. **51**, 427 (2006).
[8] J. R. Trelewicz and C. A. Schuh, Acta Mater. **55**, 5948 (2007).
[9] R. Birringer, Mater. Sci. Eng., A **117**, 33 (1989).
[10] B. Gunther, A. Kumpmann, and H. D. Kunze, Scr. Metall. Mater. **27**, 833 (1992).
[11] T. R. Malow and C. C. Koch, J. Metastable Nanocryst. Mater. **225**, 595 (1996).
[12] I. Bakonyi, E. TothKadar, L. Pogany, A. Cziraki, I. Gerocs, K. VargaJosepovits, B. Arnold, and K. Wetzig, Surf. Coat. Technol. **78**, 124 (1996).
[13] R. T. C. Choo, J. M. Toguri, A. M. Elsherik, and U. Erb, J. Appl. Electrochem. **25**, 384 (1995).
[14] H. Natter, M. Schmelzer, and R. Hempelmann, J. Mater. Res. **13**, 1186 (1998).
[15] N. S. Qu, D. Zhu, K. C. Chan, and W. N. Lei, Surf. Coat. Technol. **168**, 123 (2003).
[16] A. Robertson, U. Erb, and G. Palumbo, Nanostruct. Mater. **12**, 1035 (1999).
[17] J. A. Haber and W. E. Buhro, J. Am. Chem. Soc. **120**, 10847 (1998).
[18] F. Zhou, J. Lee, and E. J. Lavernia, Scr. Mater. **44**, 2013 (2001).
[19] N. Joshi, D. K. Aswal, A. K. Debnath, S. K. Gupta, and J. V. Yakhmi, Appl. Surf. Sci. **228**, 302 (2004).
[20] C. S. Pande and R. A. Masumura, Mater. Sci. Eng., A **409**, 125 (2005).
[21] A. J. Detor and C. A. Schuh, J. Mater. Res. **22**, 3233 (2007).
[22] F. Ebrahimi and H. Q. Li, Scr. Mater. **55**, 263 (2006).
[23] G. D. Hibbard, K. T. Aust, and U. Erb, Mater. Sci. Eng., A **433**, 195 (2006).
[24] H. Q. Li and F. Ebrahimi, Acta Mater. **51**, 3905 (2003).
[25] F. J. Humphreys and M. Hatherly, *Recrystallization and Related Annealing Phenomena* (Pergamon, Tarrytown, NY, 1995).
[26] R. Kirchheim, Acta Mater. **50**, 413 (2002).
[27] C. E. Krill, H. Ehrhardt, and R. Birringer, Z. Metallkd. **96**, 1134 (2005).
[28] J. Weissmuller, Nanostruct. Mater. **3**, 261 (1993).
[29] J. Weissmuller, J. Mater. Res. **9**, 4 (1994).
[30] J. Weissmuller, Mater. Sci. Eng., A **179**, 102 (1994).
[31] A. P. Sutton and R. W. Balluffi, *Interfaces in Crystalline Materials* (Clarendon, Oxford, 1995).
[32] J. Weissmuller, W. Krauss, T. Haubold, R. Birringer, and H. Gleiter, Nanostruct. Mater. **1**, 439 (1992).
[33] F. Liu and R. Kirchheim, J. Cryst. Growth **264**, 385 (2004).
[34] F. Liu and R. Kirchheim, Scr. Mater. **51**, 521 (2004).
[35] K. A. Darling, R. N. Chan, P. Z. Wong, J. E. Semones, R. O. Scattergood, and C. C. Koch, Scr. Mater. **59**, 530 (2008).
[36] A. J. Detor and C. A. Schuh, Acta Mater. **55**, 4221 (2007).
[37] A. J. Detor and C. A. Schuh, Acta Mater. **55**, 371 (2007).
[38] A. J. Detor, M. K. Miller, and C. A. Schuh, Philos. Mag. **86**, 4459 (2006).
[39] B. Farber, E. Cadel, A. Menand, G. Schmitz, and R. Kirchheim, Acta Mater. **48**, 789 (2000).
[40] A. J. Detor, M. K. Miller, and C. A. Schuh, Philos. Mag. Lett. **87**, 581 (2007).
[41] P. Choi, T. Al-Kassab, F. Gartner, H. Kreye, and R. Kirchheim, Mater. Sci. Eng., A 353, 74 (2003).
[42] P. C. Millett, R. P. Selvan, S. Bansal, and A. Saxena, Acta Mater. **53**, 3671 (2005).
[43] P. C. Millett, R. P. Selvam, and A. Saxena, Acta Mater. **54**, 297 (2006).
[44] P. C. Millett, R. P. Selvam, and A. Saxena, Acta Mater. **55**, 2329 (2007).

[45] K. Ishida, J. Alloys Compd. **235**, 244 (1996).
[46] Q. P. Meng, Y. H. Rong, and T. Y. Hsu, Mater. Sci. Eng., A **471**, 22 (2007).
[47] S. Swaminarayan and D. J. Srolovitz, Acta Mater. **44**, 2067 (1996).
[48] D. L. Beke, C. Cserhati, and I. A. Szabo, J. Appl. Phys. **95**, 4996 (2004).
[49] C. Cserhati, I. A. Szabo, and D. L. Beke, J. Appl. Phys. **83**, 3021 (1998).
[50] O. C. Hellman and D. N. Seidman, Mater. Sci. Eng., A **327**, 24 (2002).
[51] A. R. Miedema, Philips Tech. Rev. **36**, 217 (1976).
[52] A. R. Miedema, J. Less-Common Met. **46**, 67 (1976).
[53] A. R. Miedema, R. Boom, and F. R. Deboer, J. Less-Common Met. **41**, 283 (1975).